Gravitational Waves from Binary Black Hole Mergers inside Stars

Joseph M. Fedrow,[1,*] Christian D. Ott,[1,2] Ulrich Sperhake,[3,2] Jonathan Blackman,[2]
Roland Haas,[4] Christian Reisswig,[2] and Antonio De Felice[1]

[1]*Center for Gravitational Physics and International Research Unit of Advanced Future Studies,
Yukawa Institute for Theoretical Physics, Kyoto University, 606-8317 Kyoto, Japan*
[2]*TAPIR, Walter Burke Institute for Theoretical Physics, California Institute of Technology, Pasadena, California 91125-0001, USA*
[3]*Department of Applied Mathematics and Theoretical Physics, Centre for Mathematical Sciences, University of Cambridge,
CB3 0WA Cambridge, United Kingdom*
[4]*National Center for Supercomputing Applications, University of Illinois at Urbana-Champaign,
1205 W Clark St., Urbana, Illinois 61801, USA*

We present results from a controlled numerical experiment investigating the effect of stellar density gas on the coalescence of binary black holes (BBHs) and the resulting gravitational waves (GWs). This investigation is motivated by the proposed stellar core fragmentation scenario for BBH formation and the associated possibility of an electromagnetic counterpart to a BBH GW event. We employ full numerical relativity coupled with general-relativistic hydrodynamics and set up a $30 + 30\ M_\odot$ BBH (motivated by GW150914) inside gas with realistic stellar densities. Our results show that at densities $\rho \gtrsim 10^6$–$10^7\ \mathrm{g\,cm^{-3}}$ dynamical friction between the BHs and gas changes the coalescence dynamics and the GW signal in an unmistakable way. We show that for GW150914, LIGO observations appear to rule out BBH coalescence inside stellar gas of $\rho \gtrsim 10^7\ \mathrm{g\,cm^{-3}}$. Typical densities in the collapsing cores of massive stars are in excess of this density. This excludes the fragmentation scenario for the formation of GW150914.

Introduction.—With the recent detection of the first gravitational wave (GW) events by LIGO [1], the era of GW astronomy has begun. An extensive multiwavelength network of astronomical observatories is following up each candidate GW event with the hope of catching an electromagnetic (EM) counterpart. This is very well motivated for GWs from neutron star (NS) mergers (e.g., Ref. [2]), but for observed GWs from the merger of stellar-mass binary black holes (BBHs), no EM counterpart is expected (e.g., Ref. [3]).

However, the first observed BBH GW event, GW150914 [4], was possibly connected with a γ-ray event seen by the Fermi satellite [5] (though note it was not observed by other γ-ray satellites [6,7]). If directly related, this would be a totally unexpected EM counterpart to what was believed to be a BBH merger in pure vacuum.

To explain such an EM counterpart, Loeb [8] proposed that the coalescing BHs formed via dynamical fragmentation in a very massive star undergoing gravitational collapse. This scenario is tentatively supported by the simulations of Ref. [9], who found BBH formation by dynamical fragmentation in pair-unstable supermassive primordial stars. The result of Loeb's scenario would be a BBH system embedded in high-density stellar gas whose coalescence could drive outflows giving rise to the γ-ray transient observed by Fermi.

There are arguments from stellar evolution [10] suggesting it may be difficult to obtain collapsing stellar cores permitting dynamical fragmentation. However, this possibility is not conclusively ruled out by theory.

In this Letter, we consider the scenario in which a BBH was formed inside a collapsing massive star and conduct the first numerical relativity simulations of BBH mergers in the presence of gas with densities comparable to those in the cores of collapsing massive stars. The results of our simulations show that the GWs observed from GW150914 *are inconsistent* with this event having taken place inside a collapsing massive star, ruling out the dynamical fragmentation scenario.

Methods and initial data.—We employ the open-source EINSTEIN TOOLKIT and evolve Einstein's equations in the Baumgarte-Shapiro-Shibata-Nakamura formalism [11,12] with fourth-order finite differences and adaptive mesh refinement (AMR). We include general-relativistic (GR) hydrodynamics in the finite-volume approach with piecewise parabolic reconstruction at cell interfaces and the Marquina flux formula for intercell fluxes [13]. Inside the BH apparent horizons, we correct unphysical states using the methods detailed in Refs. [14,15]. Spacetime and hydrodynamics evolution are coupled in a fourth-order Runge-Kutta integrator.

For generality, we describe our setup in $G = c = 1$ units and measure quantities in terms of the Arnowitt-Deser-Misner mass M. We employ BBH puncture initial data and carry out a vacuum simulation (model G0) and four simulations in which we embed the BBH system in gas of constant density $\rho_0 = \{10^{-10}, 10^{-9}, 10^{-8}, 10^{-7}\}\ M^{-2}$ initially at rest, labeled G1–G4 in the order shown. We use TwoPUNCTURES [16,17] to solve for constraint satisfying quasicircular initial data, taking

into account the gas, and placing the two equal-mass, nonspinning punctures at a coordinate separation of $11.6\,M$. In the vacuum case, this corresponds to 8 orbits to merger. We employ a Γ-law equation of state $P = (\Gamma - 1)\rho\epsilon$ for the gas. We set $\Gamma = 4/3$ and obtain the initial ϵ by assuming a gas dominated by relativistic degenerate electrons (e.g., Ref. [18]). We smoothly reduce ρ to an atmosphere value of $10^{-16}\,M^{-2}$ outside of $80\,M$ by applying $X(R) = 0.5[1 + \tanh([R - 80\,M]/15\,M)]$.

We employ seven levels of AMR with the outer boundary placed at $320\,M$. The punctures are covered with a finest grid of $\Delta x = 0.0195\,M$, which corresponds to approximately 45 grid points across each apparent horizon after an initial gauge adjustment. The fine grid has a linear extent of $3\,M$ to provide high resolution for the gas dynamics near the horizons. It is embedded in five coarser AMR levels tracking the punctures' orbital motion. The outermost two levels are fixed. We extract GWs at $R = 120\,M$ where $\Delta x = 0.625\,M$ using the Newman-Penrose Ψ_4 formalism [19,20]. We obtain the GW strain via fixed-frequency integration [21].

Rescaled to a BBH mass of $M = 60\,M_\odot$ for comparison with GW150914, each puncture has an approximate initial mass of $30\,M_\odot$, the initial separation is 1030 km, with gas densities $\rho_0 = 1.72 \times \{10^4, 10^5, 10^6, 10^7\}\,\mathrm{g\,cm^{-3}}$. The typical central density in a presupernova star is 10^9–$10^{10}\,\mathrm{g\,cm^{-3}}$. At a radius of 1000 km it is in the range 10^7–$10^9\,\mathrm{g\,cm^{-3}}$, depending on stellar mass (e.g., Ref. [22]). We choose $10^7\,\mathrm{g\,cm^{-3}}$ as the highest simulated density since it is a reasonable and arguably low value for the density of outer stellar core material left surrounding the BBH formed in dynamical fragmentation. With the above choices, the total gas mass on the computational grid is $\sim 13.8[M/(60\,M_\odot)][\rho_0/(1.72 \times 10^7\,\mathrm{g\,cm^{-3}})]\,M_\odot$.

We provide a convergence study and analysis details in the Supplemental Material [23] to this Letter.

Dynamics.—In Fig. 1, we show orbital-plane snapshots of the rest-mass density at various times in model G3's coalescence. In cgs units and for the $M = 60\,M_\odot$ case, its merger time is ~ 390 ms (we define merger time based on the peak amplitude of the (2,2) GW mode). That is ~ 142 ms faster than the pure-vacuum case G0.

The density colormaps in Fig. 1 reveal that soon after the start of the simulation, an ellipsoidal high-density structure surrounds the BHs. The central high-density band visually connecting the BHs is due to the gravitational focusing of gas into this region, where acceleration toward one BH is partially cancelled by the other. This feature was also observed in BBH mergers in very low-density gas (e.g., Refs. [15,24] and references therein).

The ellipsoidal structure surrounding the BBH in Fig. 1 forms because each BH accelerates the surrounding gas, dragging it along in its gravitational wake. The associated drag force, closely related to dynamical friction (e.g., Refs. [25–30]), converts orbital energy into kinetic energy
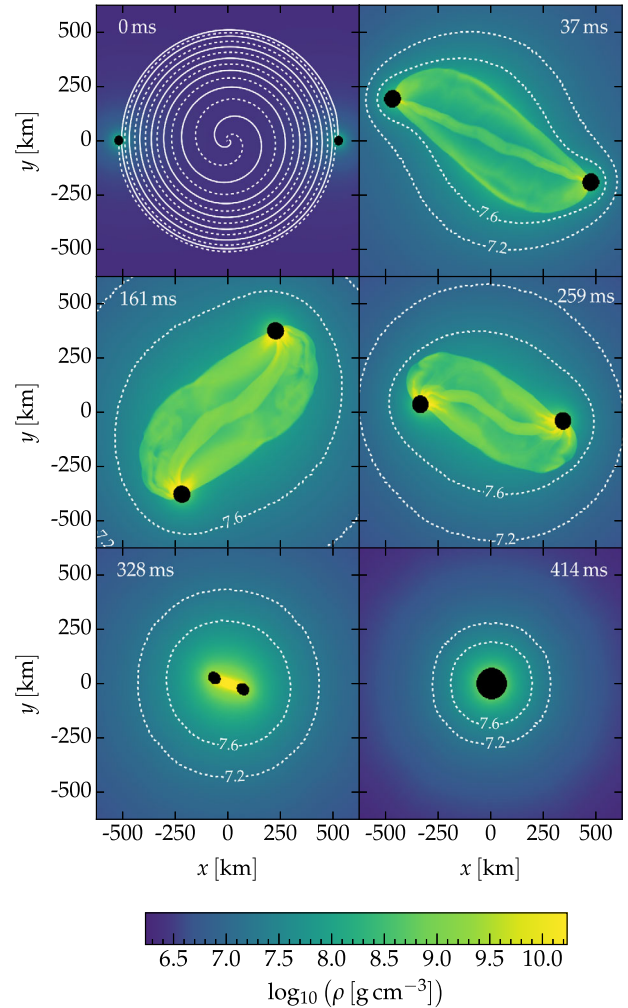

FIG. 1. BBH inspiral evolution and orbital plane density slices of the G3 model ($\rho_0 \sim 10^6\,\mathrm{g\,cm^{-3}}$). The top-left frame shows the orbital tracks followed by the BBH in the subsequent frames. The top-right frame shows the emergence of a high-density gas bar due to gravitational focusing of gas between the BHs. We choose representative isocontours at $\rho = 10^{7.2}$ and $10^{7.6}\,\mathrm{g\,cm^{-3}}$ to visualize the formation of ellipsoidal density structures surrounding the BBH. Initially, the orbital separation a decreases slowly. Gas accumulates around the BBH pushing the isocontours to larger radii (center-left frame). Once a decreases rapidly, the contours contract and circularize (center-right frame, bottom-left frame). The bottom-right frame shows the final merged BH evolving toward steady-state Bondi-Hoyle accretion.

and internal energy of the gas (through compression and shocks). This process is what rapidly robs the BBH of its orbital energy and angular momentum. It leads to an accelerated decline of the orbital separation and an earlier merger compared to the vacuum case G0.

The BHs accrete gas during coalescence, but even in the high-density G4 case, the total mass accreted by each BH is only $\sim 4\%$ of its initial mass. The effect of the gradually changing mass on the coalescence is much smaller than that of dynamical friction.

TABLE I.　Model summary. ρ_0 is the initial gas density, t_{merge} the merger time, and $\mathcal{M}_{\mathrm{ZDHP}}$ and $\mathcal{M}_{150914}$ are the GW mismatches with the vacuum waveform for Advanced LIGO design noise and noise at the time of GW150914, respectively. For GW150914, a mismatch $\mathcal{M} \gtrsim 0.0017$ becomes noticeable.

Model	$\rho_0 (M/60\,M_\odot)^{-2}$ [g cm^{-3}]	t_{merge} [ms]	$\mathcal{M}_{\mathrm{ZDHP}}$	$\mathcal{M}_{150914}$
G0 Vacuum	0	510	0	0
G1	1.72×10^4	508	8×10^{-5}	3×10^{-5}
G2	1.72×10^5	490	0.0058	0.0016
G3	1.72×10^6	369	0.1882	0.0665
G4	1.72×10^7	186	0.3718	0.2386

In Table I, we summarize key properties, including the merger times, for all simulated models. The top panel of Fig. 2 shows the BBH coordinate separation a as a function of simulation time. With increasing gas density, the merger is driven to earlier times. Model G1 ($\rho_0 \sim 10^4$ g cm^{-3}) is only very mildly affected, merging some $\Delta t \sim 2$ Ms earlier than the vacuum case G0. Δt is ~ 20 ms, ~ 142 ms, and ~ 324 ms, for models G2, G3, and G4, respectively, which have 10, 100, and 1000 times higher density than model G1. The effect of the gas on the coalescence time is thus roughly linear in density for the lower-density cases. This is qualitatively reproduced by a simple Newtonian point-particle model including GW ($\partial a/\partial t \propto a^{-3}$) and dynamical friction ($\partial a/\partial t \propto a^{5/2}$) [25] terms for orbital evolution. At high density, i.e., going from G3 to G4, dynamical friction is so strong that it is no longer a linear perturbation to the GW-dominated inspiral. The point-particle model shows that in G1–G3, the dynamical friction term is always subdominant. In G4, it initially dominates over the GW term, but quickly decreases in relevance as the orbit shrinks and GW-driven evolution takes over.
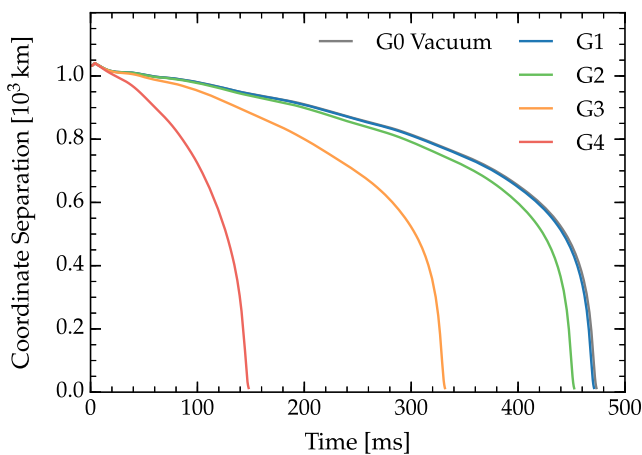

FIG. 2.　BBH coordinate separation a as a function of time until common horizon formation. All simulations start from the same separation of 1030 km (assuming a total BBH mass of 60 $M_\odot$). As ρ_0 increases across models G1–G4, dynamical friction dissipates orbital energy resulting in earlier mergers.

Gravitational waves.—In Fig. 3, we present h_+^{22}, the real part of the $l = 2$, $m = 2$ GW mode. The low density in model G1 has a negligible effect and its waveform is essentially identical to vacuum GWs. As the density increases from G1 to G4, merger occurs progressively earlier. This leads to dramatic changes in the emitted GW train and creates an unmistakable GW signature. (1) Since all models start at the same separation, the initial GW frequency is $f_0 \sim 26$ Hz for all models. (2) Dynamical friction shortens the inspiral, leading to a faster sweep ("chirp") of the GWs through frequency space. (3) The faster chirp is not due to a substantial increase of the BBH mass. Hence, merger and ringdown GW emission is at frequencies that change only mildly with ρ_0. Model G0 has a final BH mass of ~ 57.6 $M_\odot$, a dimensionless spin $a^\star = 0.69$, and we find a ringdown GW frequency of ~ 296 Hz. The highest-density model G4 produces a merged BH of ~ 64.8 $M_\odot$ and $a^\star = 0.65$, consistent (see, e.g., Ref. [31]) with its ringdown GW frequency of ~ 265 Hz.
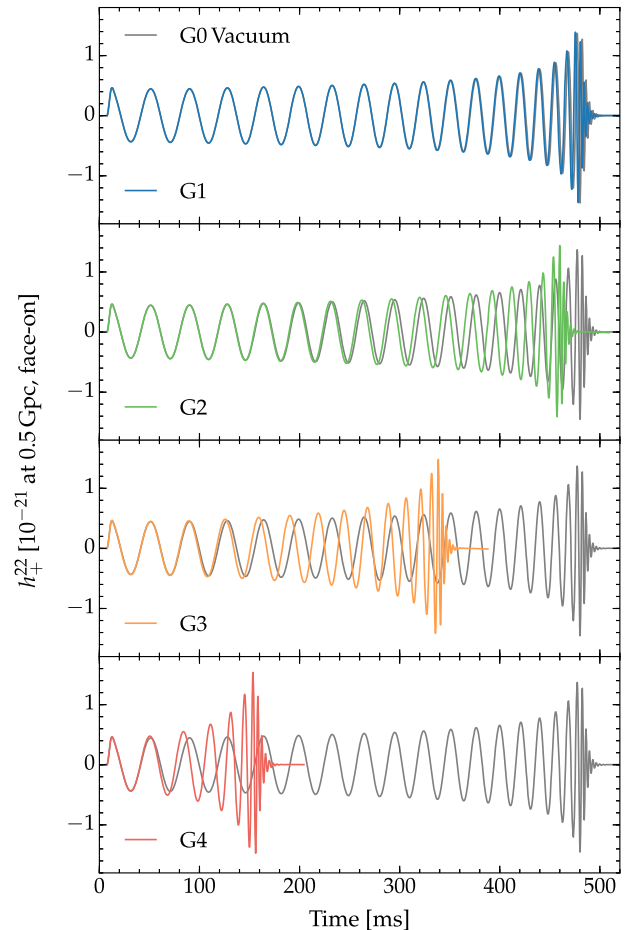

FIG. 3.　Real part of the (2,2) GW strain, observed face-on from a distance of 0.5 Gpc for a total BBH mass of 60 $M_\odot$. We compare models G1–G4 with G0 vacuum plotted in gray in each panel. All GWs start with $f \sim 26$ Hz. Increasing density leads to faster chirps. The ringdown frequency is ~ 296 Hz for G0 vacuum, decreasing by only $\sim 10\%$ for G4.

Analysis and observational consequences.—We compute the GW mismatch $\mathcal{M}(h_i, h_j)$ (see Refs. [21,32] and Supplemental Material [23]) for each waveform G1–G4 with the G0 vacuum case. GW mismatch takes into account the detector noise spectrum and we consider frequencies in the interval [26, 3000] Hz. We employ Advanced LIGO design noise [33] ($\mathcal{M}_{ZDHP}$) and the noise around GW150914 [4] ($\mathcal{M}_{150914}$). $\mathcal{M}$ is in [0, 1] and $\mathcal{M} = 0$ means h_i and h_j are identical. For an observation with signal-to-noise ratio ϱ, an $\mathcal{M} \gtrsim 1/\varrho^2$ leads to observational inconsistencies (see Ref. [34] and Supplemental Material [23] containing references [35–38]). GW150914 was observed with $\varrho \sim 24$, so $\mathcal{M} \gtrsim 0.0017$ will become noticeable.

We summarize $\mathcal{M}_{ZDHP}$ and $\mathcal{M}_{150914}$ for all models in Table I. The results for $\mathcal{M}_{150914}$ show that for GW150914, densities $\rho_0 \lesssim 10^4$ g cm^{-3} (G1) are indistinguishable from vacuum. Model G2 ($\rho_0 \sim 10^5$ g cm^{-3}) is marginally distinguishable. The situation is very different for models G3 and G4 with $\mathcal{M}_{150914} \sim 0.07$ and ~ 0.24, respectively. These results show that stellar densities $\rho_0 \gtrsim 10^6$ g cm^{-3} lead to highly significant inconsistencies with vacuum.

An additional possibility is that the G1–G4 waveforms could have lower mismatch with vacuum waveforms of BBHs with different parameters. We explore this with a seven-dimensional numerical relativity surrogate GW model [39,40], covering BBH mass ratio q (up to $q = 2$) and six spin components (up to effective spin $\chi_{eff} = (M_1 a_1^* + M_2 a_2^*)/M = 0.8$), assuming zero eccentricity. We vary parameters to minimize $\mathcal{M}_{150914}$ and find 0.011 and 0.061, for model G3 and G4, respectively. For G3, the minimum $\mathcal{M}_{150914}$ is at $M = 70.6$ $M_\odot$, $q \simeq 1.0$, and effective spin $\chi_{eff} \simeq 0.17$. For G4, we find $M = 75.3$ $M_\odot$, $q \simeq 1.6$, and $\chi_{eff} \simeq -0.47$. Even with the reduction in $\mathcal{M}_{150914}$, $\rho_0 \gtrsim 10^7$ g cm^{-3} leads to observable differences with any waveform covered by the surrogate model.

Having established that an equal mass, nonspinning BBH merger in stellar-density gas with $\rho_0 \gtrsim 10^7$ g cm^{-3} is inconsistent with GW150914 and all BBH waveforms from our surrogate model, there remains the following crucial question: Are there BBH parameter choices that could make a merger in gas appear just like GW150914?

We argue that the answer is "no": The observational BBH parameter space encompasses total mass, mass ratio, eccentricity, and six spin components. (i) BBHs of lower M inspiral to higher frequencies and have more cycles from ~ 26 Hz to merger. Using the surrogate, we find that $M = 43.7$ $M_\odot$ extends the G0 case by ~ 324 Ms, the difference in merger times between G0 and G4. However, its time-frequency evolution and ring-down frequency (~ 400 Hz) are substantially different from GW150914, leading to large mismatch. (ii) Dynamical fragmentation in our scenario leads to near-equal-mass fragments (e.g., Ref. [9]). We consider $q = 2$ as an extreme limit. In the vacuum case, it extends the inspiral by ~ 38 ms [40], insufficient to compensate for the gas effect. (iii) High

BH spin causes "orbital hangup." The effect is largest for equal spins aligned with the orbital angular momentum. Using our surrogate and the SpEC waveforms [41], we find that for $a^* = 0.99$ ($a^* = 0.4$), inspiral is prolonged by 177 ms (71 ms). The effect is linear in a^*. To explore the effect of spin in the stellar-density G4 case, we carry out a simulation with $a^* = 0.4$ for both BHs. We find that merger is delayed by ~ 17.2 ms. Extrapolating to $a^* = 0.99$ from the vacuum case, spin could extend the G4 inspiral by at most ~ 39 ms. This is insufficient to mimic GW150914.

Discussion and conclusions.—Fragmentation of a massive star's core into clumps that collapse further to NSs or BHs is an interesting scenario for the formation of NS binaries and BBHs (e.g., Refs. [9,42–44]). While perhaps unlikely (e.g., Refs. [10,45]), this scenario has not previously been ruled out observationally. As proposed by Loeb [8], it would endow a BBH merger with the gas necessary to produce an EM counterpart. Dai *et al.* [28] suggested, but did not show, that the gas surrounding the BBH could have observable consequences in the emitted GWs.

We employed numerical relativity coupled with GR hydrodynamics for a controlled experiment into the effects of stellar-density gas on BBH mergers. Scaled to a total system mass of 60 $M_\odot$ (consistent with GW150914), our results show that dynamical friction between the BHs and gas at stellar densities $\rho_0 \gtrsim 10^6$–10^7 g cm^{-3} profoundly affects the coalescence dynamics, drastically shortening the time to merger. This modifies the resulting GW signal in an unmistakable way, leading to differences with vacuum waveforms that can be observed by LIGO.

Our analysis furthermore suggests that it is not possible to choose BBH parameters that would yield a waveform in stellar-density gas resembling GW150914[46]. Thus we conclude that it is highly unlikely that GW150914 was formed through dynamical fragmentation in a massive star and Loebs scenario [8] is ruled out by the GW observation alone.

Future work should address the limitations of our work: We assumed the gas to be nonmagnetized and initially at rest, but angular momentum and magnetic fields can have dynamical impact. We employed a constant density, but real stars have radially varying density. Finally, we used a Γ-law equation of state, ignoring microphysics such as electron capture, neutrinos, and nuclear dissociation, which all may have effects on the gas dynamics. In our analysis, we did not consider GW detector calibration uncertainties of $\sim 10\%$ [4]. This should affect all waveforms equally and is unlikely to alter our conclusions.

We provide waveforms and additional visualizations of our simulations in Ref. [47].

---

*jfedrow@yukawa.kyoto-u.ac.jp

[1] B. P. Abbott *et al.*, Phys. Rev. X **6**, 041014 (2016).
[2] B. D. Metzger and E. Berger, Astrophys. J. **746**, 48 (2012).
[3] B. P. Abbott *et al.*, Astrophys. J. Lett. **826**, L13 (2016).
[4] B. Abbott *et al.*, Phys. Rev. Lett. **116**, 061102 (2016).
[5] V. Connaughton *et al.*, Astrophys. J. Lett. **826**, L6 (2016).
[6] B. Abbott *et al.*, Astrophys. J. Lett. **826**, L13 (2016).
[7] K. Hurley *et al.*, Astrophys. J. Lett. **829**, L12 (2016).
[8] A. Loeb, Astrophys. J. Lett. **819**, L21 (2016).
[9] C. Reisswig, C. D. Ott, E. Abdikamalov, R. Haas, P. Mösta, and E. Schnetter, Phys. Rev. Lett. **111**, 151101 (2013).
[10] S. Woosley, Astrophys. J. Lett. **824**, L10 (2016).
[11] M. Shibata and T. Nakamura, Phys. Rev. D **52**, 5428 (1995).
[12] T. W. Baumgarte and S. L. Shapiro, Phys. Rev. D **59**, 024007 (1998).
[13] M. A. Aloy, J. M. Ibáñez, J. M. Martí, and E. Müller, Astrophys. J. Suppl. Ser. **122**, 151 (1999).
[14] J. A. Faber, T. W. Baumgarte, Z. B. Etienne, S. L. Shapiro, and K. Taniguchi, Phys. Rev. D **76**, 104021 (2007).
[15] B. D. Farris, Y. T. Liu, and S. L. Shapiro, Phys. Rev. D **81**, 084008 (2010).
[16] M. Ansorg, B. Brügmann, and W. Tichy, Phys. Rev. D **70**, 064011 (2004).
[17] F. Löffler, L. Rezzolla, and M. Ansorg, Phys. Rev. D **74**, 104018 (2006).
[18] L. S. Shapiro and S. A. Teukolsky, *Black Holes, White Dwarfs and Neutron Stars* (John Wiley & Sons, New York U. S. A., 1983).
[19] F. Löffler *et al.*, Classical Quantum Gravity **29**, 115001 (2012).
[20] E. T. Newman and R. Penrose, J. Math. Phys. (N.Y.) **3**, 566 (1962).
[21] C. Reisswig and D. Pollney, Classical Quantum Gravity **28**, 195015 (2011).
[22] S. E. Woosley, A. Heger, and T. A. Weaver, Rev. Mod. Phys. **74**, 1015 (2002).
[23] See Supplemental Material at http://link.aps.org/supplemental/10.1103/PhysRevLett.119.171103 'for a convergence study and analysis details.

[24] T. Bode, T. Bogdanović, R. Haas, J. Healy, P. Laguna, and D. Shoemaker, Astrophys. J. **744**, 45 (2012).
[25] A. Escala, R. B. Larson, P. S. Coppi, and D. Mardones, Astrophys. J. **607**, 765 (2004).
[26] S. Chandrasekhar, Astrophys. J. **97**, 255 (1943).
[27] E. C. Ostriker, Astrophys. J. **513**, 252 (1999).
[28] L. Dai, J. C. McKinney, and M. C. Miller, Mon. Not. R. Astron. Soc. **470**, L92 (2017).
[29] E. Barausse, Mon. Not. R. Astron. Soc. **382**, 826 (2007).
[30] E. Barausse, V. Cardoso, and P. Pani, Phys. Rev. D **89**, 104059 (2014).
[31] E. Berti, V. Cardoso, and A. O. Starinets, Classical Quantum Gravity **26**, 163001 (2009).
[32] T. Damour, B. R. Iyer, and B. S. Sathyaprakash, Phys. Rev. D **57**, 885 (1998).
[33] D. Shoemaker, LIGO Scientific Collaboration Technical Report LIGO-T0900288-v3, (2010), https://dcc.ligo.org/LIGO-T0900288/public.
[34] L. Lindblom, B. J. Owen, and D. A. Brown, Phys. Rev. D **78**, 124020 (2008).
[35] C. Cutler and É. E. Flanagan, Phys. Rev. D **49**, 2658 (1994).
[36] I. W. Harry and S. Fairhurst, Phys. Rev. D **83**, 084002 (2011).
[37] W. Althous, L. Jones, and A. Lazzarini, LIGO Laboratory, Technical Report LIGO-T980044-10, (1997), https://dcc.ligo.org/T980044/public.
[38] B. P. Abbott *et al.*, Phys. Rev. Lett. **116**, 241102 (2016).
[39] J. Blackman, S. E. Field, M. A. Scheel, C. R. Galley, D. A. Hemberger, P. Schmidt, and R. Smith, Phys. Rev. D **95**, 104023 (2017).
[40] J. Blackman, S. E. Field, M. A. Scheel, C. R. Galley, C. D. Ott, M. Boyle, L. E. Kidder, H. P. Pfeiffer, and B. Szilágyi, Phys. Rev. D **96**, 024058 (2017).
[41] http://www.black-holes.org/waveforms
[42] I. A. Bonnell and J. E. Pringle, Mon. Not. R. Astron. Soc. **273**, L12 (1995).
[43] M. B. Davies, A. King, S. Rosswog, and G. Wynn, Astrophys. J. Lett. **579**, L63 (2002).
[44] K. A. Postnov, A. G. Kuranov, D. A. Kolesnikov, S. B. Popov, and N. K. Porayko, Mon. Not. R. Astron. Soc. **463**, 1642 (2016).
[45] C. L. Fryer and M. S. Warren, Astrophys. J. **601**, 391 (2004).
[46] B. P. Abbott *et al.*, Classical Quantum Gravity **34**, 104002 (2017).
[47] See https://stellarcollapse.org/bbhgas.
[48] J. D. Hunter, Comput. Sci. Eng. **9**, 90 (2007).